Computers and Fluids 141 (2016) 75–81

Contents lists available at ScienceDirect

Computers and Fluids

journal homepage: www.elsevier.com/locate/compfluid

On three-dimensional ALE finite element model for simulating deformed interstitial medium in the presence of a moving needle

Yannick Deleuze [a,b,*], Marc Thiriet [a,c,d], Tony W.H. Sheu [b,e]

[a] Sorbonne Universités, UPMC Univ Paris 06, UMR 7598, Laboratoire Jacques-Louis Lions, F-75005, Paris, France
[b] Department of Engineering Science and Ocean Engineering, National Taiwan University, No. 1, Sec. 4, Roosevelt Road, Taipei, Taiwan
[c] CNRS, UMR 7598, Laboratoire Jacques-Louis Lions, F-75005, Paris, France
[d] INRIA-Paris-Rocquencourt, EPC REO, Domaine de Voluceau, BP105, 78153 Le Chesnay Cedex, France
[e] Center for Advanced Study in Theoretical Sciences, National Taiwan University, No. 1, Sec. 4, Roosevelt Road, Taipei, Taiwan

ARTICLE INFO

Article history:
Received 30 September 2015
Revised 25 July 2016
Accepted 4 August 2016
Available online 4 August 2016

Keywords:
Finite element method
ALE
FreeFem++
Acupuncture
Brinkman model
Interstitial fluid flow

ABSTRACT

The effect of inserted needle on the subcutaneous interstitial flow is studied. Our goal is to describe the physical stress affecting cells during acupuncture needling. The convective Brinkman equations are considered to describe the flow through a fibrous medium. Three-dimensional simulations are carried out by employing an ALE finite element model. Numerical studies illustrate the acute physical stress developed by the implantation of a needle.

1. Introduction

In recent years, computational techniques have been widely used by researchers to investigate and simulate biological flow within three dimensional context. Applications include blood flow models, air flow models in the respiratory tract, interstitial flow models, and chemical mediators transport. Most of the structure and fluid interactions have been considered with simplified rigid wall or deformable wall models.

Methods to predict flows that account for moving domains or domain deformability using the finite element method are based on fixed mesh methods or moving mesh methods. On the one hand, fixed mesh methods include the immersed boundary formulation [1] which relies on the description of solid phase by adding a force vector to the governing equations. A similar approach, known as the fictitious domain formulation [2,3], is based on the use of Lagrange multipliers to enforce kinematic condition on the solid phase or alternatively based on a penalty method [3]. Both methods track solid phase with a characteristic function or a level set function. These methods are well adapted to moving bodies in the fluid or fluid-structure computation with interface of a highly geometric complexity. The latest method has been implemented with FreeFem++ [4]. On the other hand, moving mesh methods include the Lagrangian method, the moving finite element (MFE) method [5,6], the deformation map method [7], the Geometric Conservation Law (GCL) method [8], the space/time method [9–12], and the Arbitrarily Lagrangian–Eulerian (ALE) method [13–15] for the solution of fluid dynamic problems. Note that the space-time finite element method can also be implemented in FreeFem++ in 1D and 2D.

Significant progress has been made in recent years in solving fluid-structure interaction problems in deformable domains using the ALE method. The mathematically rigorous ALE framework has been well accepted to be applicable to simulate transport phenomena in time and allows some freedom in the description of mesh motion. A theoretical analysis of the ALE method can be found in [16,17]. However, ALE equations are computationally expensive when considering a large domain because of the necessity of continuously updating the geometry of the fluid and structural mesh. Interface tracking with time discretization also raises some implementation questions. The implementation of the ALE method can be done in FreeFem++ [18].

Study of biological flows plays a central role in acupuncture research. For a description of the underlying acupuncture

* Corresponding author.
E-mail addresses: yannick.deleuze@ljll.math.upmc.fr (Y. Deleuze), marc.thiriet@upmc.fr (M. Thiriet), twhsheu@ntu.edu.tw (T.W.H. Sheu).

http://dx.doi.org/10.1016/j.compfluid.2016.08.001
0045-7930/

mechanism, one can refer to [19–21]. Interstitial flow models take into account interstitial fluid, cell membrane interaction, and fiber interactions [22]. Mastocytes, among other cells, are able to respond to fluidic stimuli via mechanotransduction pathways leading to the degranulation and liberation of chemical mediators [23]. Degranulation mechanisms include interaction of the cell membrane with interstitial and cytosolic flow [24]. Ion transport in narrow ion channels is another challenging task to model. Indeed, degranulation of chemical mediators upon stimulation can be triggered by a rapid Ca^{2+} entry in the cytosol [25].

Modeling the three-dimensional interstitial flow in tissues is extremely challenging for a large number of reasons: a complex geometry of the tissue, an accurate constitutive description of the behavior of the tissue, and flow rheology are only few examples. Macroscopic models developed for incorporating complex microscopic structure are essential for applications [22,25–28]. In the context of acupuncture, the interstitial flow has been modeled by the Brinkman equations in two-dimensional fixed domain [27,28] and two-dimensional deformable domain [19].

In this paper, a porous medium formulation of the interstitial fluid is presented for modeling mastocyte-needle interaction in deformable connective tissues. This formulation is based on the conventional ALE characteristic/Galerkin finite element model for an unsteady flow thought a porous medium modeled by the incompressible Brinkman's equations in a three-dimensional moving domain. The motion of the needle in the fluid is taken into account. The main features of the model can be summarized as follows:

1. The loose connective tissue of the hypodermis is constituted of scattered cells immersed in extracellular matrix. The extracellular matrix contains relatively sparse fibers and abundant interstitial fluid. The interstitial fluid contains water, ions and other small molecules. Such a fluid corresponds to plasma without macromolecules and interacts with the ground substance, thereby forming a viscous hydrated gel that can stabilize fiber network [29,30].
2. The Darcy law is used to approximate fibers of the media as a continuum and allows us to compute the actual microscopic flow phenomena that occur in the fibrous media.
3. Brinkman's law then allows us to describe the flow field around solid bodies such as the embedded cells in extracellular matrix.
4. Transient convective Brinkman's equations [31–33] are applied to simulate interstitial flow in a fibrous medium driven by a moving needle [19].

Although the previously stated approach cannot give information on microscopic events, it can describe macroscale flow patterns in porous media. Focus is given to the effects of interstitial fluid flow during implantation of an acupuncture needle until the tip has reached the desired location within the hypodermis. The objective of this work is to give a description of the physical stress (shear stress and pressure) influencing tissue and cells.

2. Methods

On a microscopic scale, the interstitial tissues are composed of fluid, cells, and solid fibers. The interstitial fluid contains water, ions and other small molecules. Such a fluid corresponds to plasma without macromolecules [22]. It interacts with the ground substance to form a gel-like medium.

A model taking into account individual fibers and cell adhesion complexes is already a falsification of the reality. Moreover, it is very costly from the computational viewpoint. When considering an organized homogeneous matrix of fibers, computation of such a model shows the microscopic fluctuations of the fluid shear stress at the protein level [34].

Due to biological complexity, the interstitium is considered as a fluid-filled porous material [22]. The interstitial flow is simulated using the incompressible convective Brinkman equation. The phenomenological model cannot give information on unneeded microscopic events but the Darcy equation can describe macroscale flow patterns in porous media.

2.1. Flow equations

The governing equations of the unsteady flow of an incompressible fluid through a porous medium (with mass density ρ, dynamic viscosity μ, and kinematic viscosity $\nu = \mu/\rho$) can be derived as [31–33]:

$$\frac{\rho}{\alpha_f}\left(\frac{\partial \bar{\mathbf{u}}}{\partial t} + \bar{\mathbf{u}}\cdot\nabla\left(\frac{\bar{\mathbf{u}}}{\alpha_f}\right)\right) - \mu\nabla^2\bar{\mathbf{u}} + \frac{1}{\alpha_f}\nabla(\alpha_f p_f) = -\frac{\mu}{P}\bar{\mathbf{u}} \quad \text{in } \Omega(t), \tag{1}$$

$$\nabla\cdot\bar{\mathbf{u}} = 0, \tag{2}$$

$$\bar{\mathbf{u}}(\mathbf{x}, 0) = \bar{\mathbf{u}}_0(\mathbf{x}), \tag{3}$$

where $-\frac{\mu}{P}\bar{\mathbf{u}}$ denotes the Darcy drag, P the Darcy permeability, $\bar{\mathbf{u}}$ the averaged velocity vector, and p_f the pressure. The averaged velocity is defined as

$$\bar{\mathbf{u}} = \alpha_f \mathbf{u}_f, \tag{4}$$

where $\mathbf{u}_f$ is the fluid velocity and

$$\alpha_f = \frac{\text{fluid volume}}{\text{total volume}} \tag{5}$$

is the fluid volume fraction. This volume fraction corresponds to the effective porosity of the medium. The fluid fractional volume α_f is taken as a space-dependent parameter to model the distinguished properties around an acupoint.

The system of equations (1–2) is applied to the case of a flow driven by the motion of a needle in the deformable domain $\Omega(t)$ [19]. The domain boundary can be decomposed into four surfaces: the needle boundary denoted by Γ_1, an impervious boundary (wall) denoted by Γ_2, the mastocyte membrane denoted by Γ_3, and the open boundary on the sides denoted by Γ_4. The classical no-slip condition is applied to the needle surface Γ_1, the rigid wall Γ_2, and the cell surface Γ_3. At the outer boundary Γ_4 a traction-free boundary condition is prescribed. Thus, the entire set of boundary conditions reads as

$$\bar{\mathbf{u}} = \mathbf{v}_{\text{needle}}, \text{ on } \Gamma_1, \tag{6}$$

$$\bar{\mathbf{u}} = 0, \text{ on } \Gamma_2, \tag{7}$$

$$\bar{\mathbf{u}} = 0, \text{ on } \Gamma_3, \tag{8}$$

$$-\mu\nabla\bar{\mathbf{u}}\cdot\mathbf{n} + p_f\mathbf{n} = 0, \text{ on } \Gamma_4. \tag{9}$$

2.2. Finite element model

The governing equations in Section 2.2.1 are solved using the finite element software FreeFem++ [35]. This code programs the discrete equations derived from the finite element weak formulation of the problem presented in Section 2.2.3 using a characteristic/Galerkin model to stabilize convection terms.

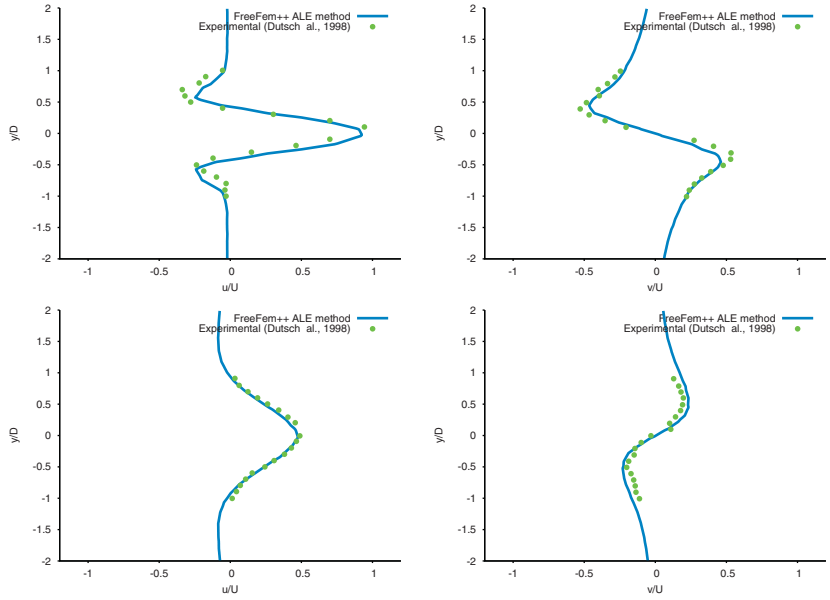

Fig. 1. Comparison of the computed and referenced solutions along the line $x = -0.6 * D$ (top) and $x = 1.2 * D$ (bottom) for the values of $\mathbf{u} = (u, v)$ at $t = \frac{55}{12}T$.

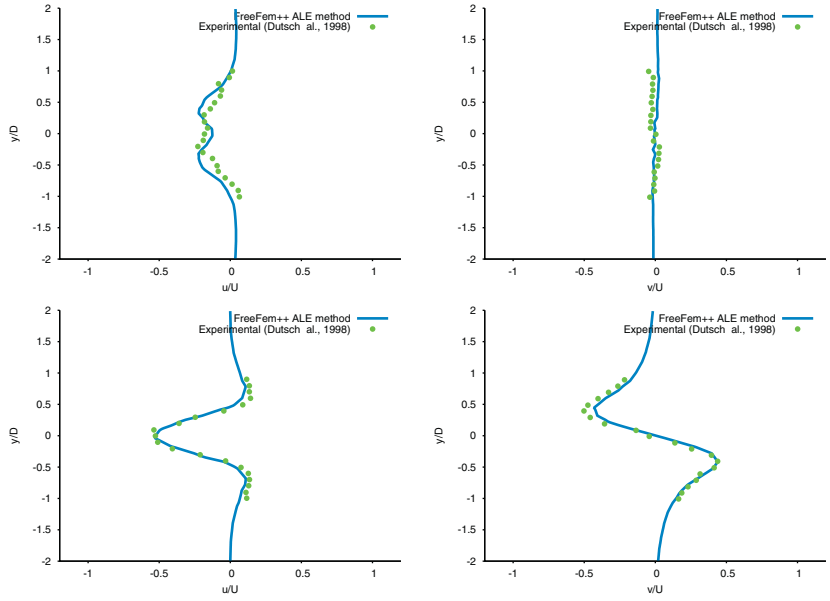

Fig. 2. Comparison of the computed and referenced solutions along the line $x = -0.6 * D$ (top) and $x = 1.2 * D$ (bottom) for the values of $\mathbf{u} = (u, v)$ at $t = \frac{59}{12}T$.

2.2.1. Scaling and setting for numerical simulations

L denotes the characteristic length that is the needle width and V is the characteristic velocity set to be the needle maximum velocity. Rescaling the variables leads to

$$\mathbf{x}' = \frac{\mathbf{x}}{\mathrm{L}}, \quad t' = \frac{t}{(\mathrm{L}/\mathrm{V})}, \quad p' = \frac{p_f}{(\rho V^2)}, \quad \mathbf{u}' = \frac{\tilde{\mathbf{u}}}{\mathrm{V}}. \tag{10}$$

In the resulting dimensionless form, after removing the prime in the rescaled variables, the dimensionless incompressible convective Brinkman equations read as

$$\frac{1}{\alpha_f}\frac{\partial \mathbf{u}}{\partial t} + \frac{1}{\alpha_f}\mathbf{u}\cdot\nabla\left(\frac{\mathbf{u}}{\alpha_f}\right) - \frac{1}{\mathrm{Re}}\nabla^2\mathbf{u} + \frac{1}{\alpha_f}\nabla(\alpha_f p) = -\frac{1}{\mathrm{Da}\,\mathrm{Re}}\mathbf{u}, \tag{11}$$

$$\nabla\cdot\mathbf{u} = 0. \tag{12}$$

where Re is the Reynolds number and Da is the Darcy number. The previous dimensionless parameters are defined as

$$\mathrm{Re} = \frac{\rho \mathrm{L}\mathrm{V}}{\mu}, \quad \mathrm{Da} = \frac{P}{\mathrm{L}^2}. \tag{13}$$

In considering the above dimensionless governing equations, the normalized boundary conditions on the domain boundary are prescribed as

$$\mathbf{u} = \mathbf{v} \quad \text{on } \Gamma_1, \tag{14}$$

$$\mathbf{u} = 0 \quad \text{on } \Gamma_2, \tag{15}$$

$$\mathbf{u} = 0 \quad \text{on } \Gamma_3, \tag{16}$$

$$-\frac{1}{\mathrm{Re}}\nabla\mathbf{u}\cdot\mathbf{n} + p\mathbf{n} = 0 \quad \text{on } \Gamma_4. \tag{17}$$

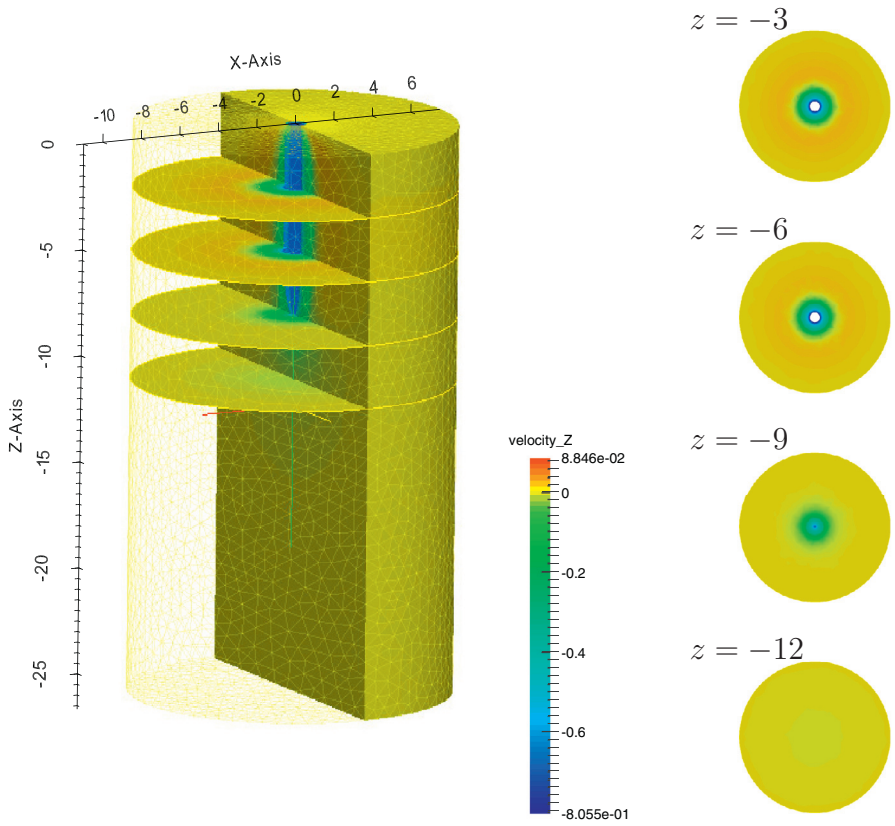

Fig. 3. The predicted contours of velocity along the z-direction resulting from the needle (blue) motion in interstitial fluid with $\alpha_f = 0.7$, $\mathrm{Da} = 0.321$, and $\mathrm{Re} = 0.103$. (For interpretation of the references to colour in this figure legend, the reader is referred to the web version of this article.)

2.2.2. ALE implementation on moving meshes

In the present paper, the ALE framework built in FreeFem++ is employed to compute the flow in the moving domain. In the current problem setting, the motion of needle is prescribed with respect to time. The boundary of the domain is thus exactly known at each time so that an area preserving mesh can be precisely generated.

The framework of the ALE approach employed is briefly described below. Let $\Omega(t)$ be the domain at each time t with regular boundary $\partial\Omega(t)$. In the Eulerian description, the fluid is described by

$$\mathbf{u}(\mathbf{x}, t) \text{ and } p(\mathbf{x}, t), \forall \mathbf{x} \in \Omega(t). \tag{18}$$

To follow a moving domain, one can define the ALE map as

$$\tilde{\mathcal{A}} : \tilde{\omega} \times \mathbb{R}^+ \to \mathbb{R}^2 \quad (\tilde{\mathbf{x}}, t) \to \tilde{\mathcal{A}}(\tilde{\mathbf{x}}, t) := \tilde{\mathcal{A}}_t, \tag{19}$$

such that $\omega(t) = \tilde{\mathcal{A}}(\tilde{\omega}, t)$, where $\tilde{\omega}$ is the reference computational domain. Given an ALE field $\tilde{q} : \tilde{\omega} \times \mathbb{R}^+ \to \mathbb{R}$, its Eulerian description is given by

$$\forall \mathbf{x} \in \Omega(t), q(\mathbf{x}, t) = \tilde{q}(\tilde{\mathcal{A}}_t^{-1}(\mathbf{x}), t) \tag{20}$$

In ALE framework, the computational domain velocity (or ALE velocity or grid velocity) is defined as

$$\tilde{\mathbf{a}}(\tilde{\mathbf{x}}, t) = \frac{\partial \tilde{\mathcal{A}}}{\partial t}(\tilde{\mathbf{x}}, t), \quad \forall \tilde{\mathbf{x}} \in \tilde{\omega}, \tag{21}$$

so that we can get

$$\mathbf{a}(\mathbf{x}, t) = \tilde{\mathbf{a}}(\tilde{\mathcal{A}}_t^{-1}, t). \tag{22}$$

The ALE time-derivative is defined as

$$\left.\frac{\partial q}{\partial t}\right|_{\tilde{\mathcal{A}}} = \frac{\mathrm{d}}{\mathrm{d}t} q(\tilde{\mathcal{A}}(\tilde{\mathbf{x}}, t), t), \tag{23}$$

and the following identity holds

$$\left.\frac{\partial q}{\partial t}\right|_{\tilde{\mathcal{A}}} = (\mathbf{a} \cdot \nabla) q + \frac{\partial q}{\partial t}. \tag{24}$$

A general method is used to construct the mapping or, equivalently, the domain velocity **a**. The domain velocity is computed by solving the following Laplace equation subjected to the Dirichlet boundary condition [36]

$$-\nabla^2 \mathbf{a} = 0, \qquad \mathbf{a}_{|_{\partial\Omega}} = \mathbf{v}. \tag{25}$$

In the ALE framework, the equations 11–(12), subject to a prescribed needle motion, become

$$\left.\frac{\partial (\mathbf{u}/\alpha_f)}{\partial t}\right|_{\tilde{\mathcal{A}}} + \left(\left(\frac{\mathbf{u}}{\alpha_f} - \mathbf{a}\right) \cdot \nabla\right) \frac{\mathbf{u}}{\alpha_f} - \frac{1}{\mathrm{Re}} \nabla^2 \mathbf{u} + \frac{1}{\alpha_f} \nabla (\alpha_f p) = -\frac{\mathbf{u}}{\mathrm{Da}\,\mathrm{Re}}, \tag{26}$$

$$\nabla \cdot \mathbf{u} = 0. \tag{27}$$

The solutions **u** and p are sought subject to the initial condition (3) and the boundary conditions 7–(9) described in Section 2.2.1.

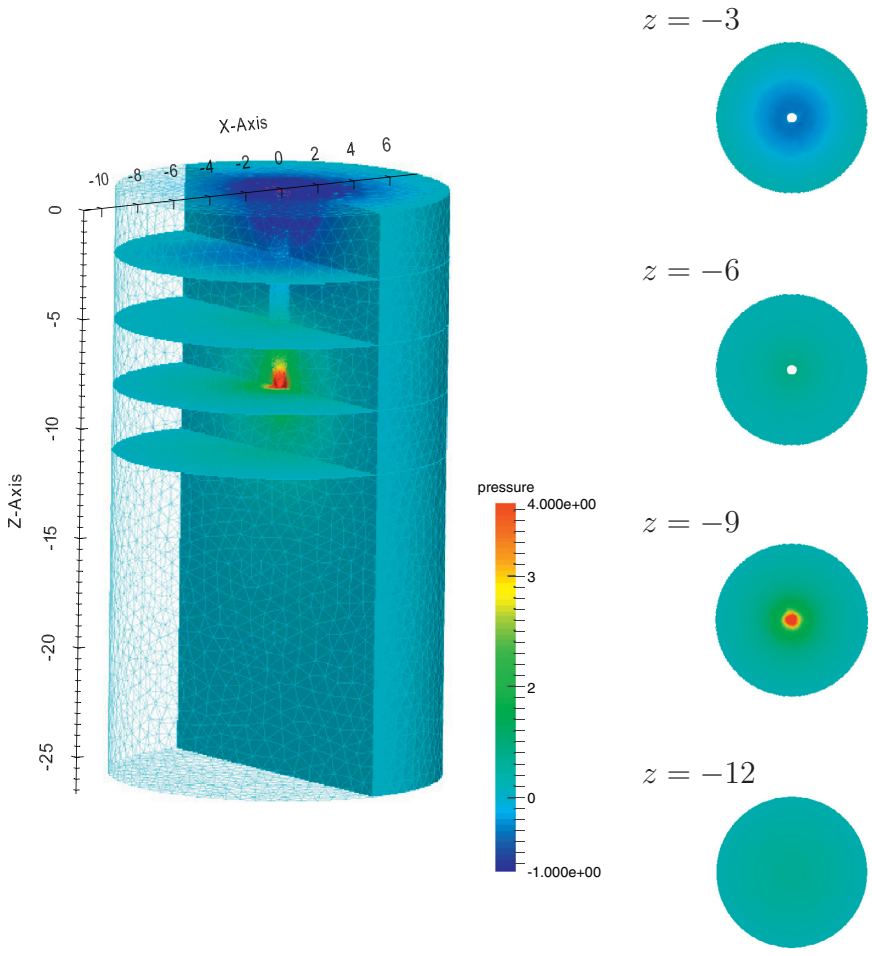

Fig. 4. The predicted contours of velocity along the z-direction resulting from the needle (blue) motion in interstitial fluid with $\alpha_f = 0.7$, Da $= 0.321$, and Re $= 0.103$. (For interpretation of the references to colour in this figure legend, the reader is referred to the web version of this article.)

2.2.3. Finite element discretization

The convective incompressible Brinkman equations are approximated with the method of characteristics for the nonlinear convection term and a Galerkin method for the rest of the spatial derivative terms. The time discretization gives

$$\frac{1}{\Delta t}\left(\frac{\mathbf{u}^{n+1}}{\alpha_f} - \left(\frac{\mathbf{u}^n}{\alpha_f}\right)\circ \mathbf{X}^n\right) - \frac{1}{\mathrm{Re}}\nabla^2\mathbf{u}^{n+1} + \frac{1}{\alpha_f}\nabla(\alpha_f p^{n+1}) = -\frac{\mathbf{u}^{n+1}}{\mathrm{Da}\,\mathrm{Re}}, \tag{28}$$

$$\nabla\cdot\mathbf{u}^{n+1} + \varepsilon p^{n+1} = 0, \tag{29}$$

in Ω^{n+1}. Note that $\mathbf{X}^n$ is approximated by $\mathbf{X}^n \approx \mathbf{x} - \left(\frac{\mathbf{u}^n}{\alpha_f} - \mathbf{a}^n\right)(\mathbf{x})\,\Delta t$. Note that a small stabilization parameter epsilon is introduced following the so-called artificial compressibility method introduced in [37] and [38].

For all $\varphi \in H^{1/2}(\Gamma_1)$, let us introduce the product space

$$V_\varphi = \left\{(\mathbf{w}, q) \in [H^1(\Omega)]^2 \times L^2(\Omega), \mathbf{w} = \varphi \text{ on } \Gamma_1, \mathbf{w} = 0 \text{ on } \Gamma_2\right\}. \tag{30}$$

Let

$$(a, b) = \int_{\Omega^{n+1}} ab\,\mathrm{d}\mathbf{x}. \tag{31}$$

The weak formulation becomes the following finite dimensional linear system: find $(\mathbf{u}^{n+1}, p^{n+1}) \in V_g$ such that

$$\begin{aligned}&\frac{1}{\Delta t}\left(\frac{\mathbf{u}^{n+1}}{\alpha_f} - \left(\frac{\mathbf{u}^n}{\alpha_f}\right)\circ\mathbf{X}^n, \mathbf{w}\right) + \frac{1}{\mathrm{Re}}\left(\frac{1}{\alpha_f}\nabla\mathbf{u}^{n+1}, \nabla\mathbf{w}\right)\\ &\quad - \left(\alpha_f p^{n+1}, \nabla\cdot\left(\frac{\mathbf{w}}{\alpha_f}\right)\right) + \frac{1}{\mathrm{Da}\,\mathrm{Re}}\left(\mathbf{u}^{n+1}, \mathbf{w}\right) = 0,\\ &\left(\nabla\cdot\mathbf{u}^{n+1}, q\right) + \varepsilon\left(p^{n+1}, q\right) = 0,\end{aligned} \tag{32}$$

for all $(\mathbf{w}, q) \in V_0$.

The Taylor–Hood $\mathbb{P}_2$–$\mathbb{P}_1$ elements are adopted to ensure satisfaction of the LBB stability condition [39]. Note that temporal accuracy order of the presented characteristic/Galerkin method is one. Meshes are generated within FreeFem++ and mesh adaptation is performed prior to simulations so as to improve mesh quality around the needle and the cell.

2.3. Validation

Let the interaction of an oscillating circular cylinder with a fluid at rest be considered. The problem is to find the velocity vector field $\mathbf{u}$ and the pressure p of a flow satisfying the incompressible Navier–Stokes equations in the domain $\Omega = [-l, l] \times [-h, h]$ with no-slip boundary conditions on the cylinder and traction-free boundary condition on the border of the physical domain.

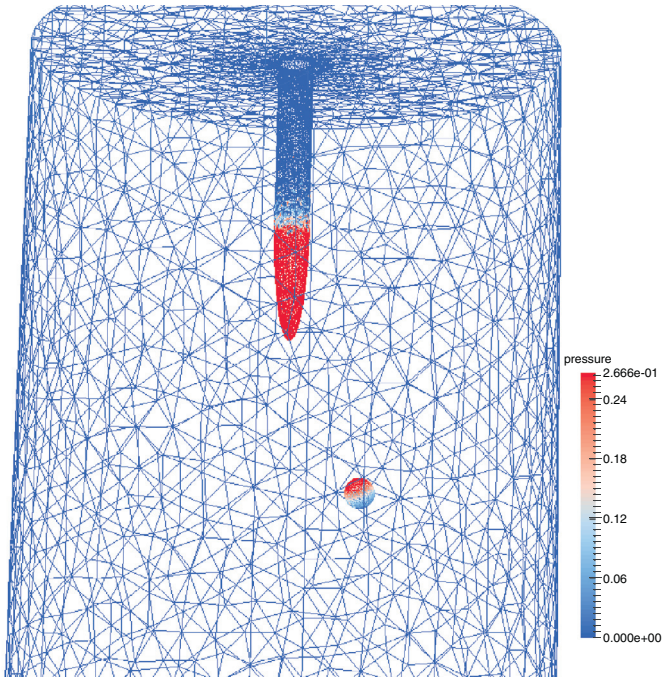

Fig. 5. The predicted pressure contours on the needle and cell surface as the needle moves toward the cell with $\alpha_f = 0.7$, Da $= 0.321$, and Re $= 0.103$.

The horizontal velocity of the cylinder of diameter D is given by $u_c(t) = -U\cos(2\pi f t)$, where $U = 2\pi A f$. At each time step, the mesh is moved according to the displacement $\mathbf{a}\,\Delta t$, where $\mathbf{a}$ is the solution of (25). As soon as the mesh is moved, the computed $\mathbf{a}^n$ and $\mathbf{u}^n$, that are defined in the previous mesh, are then pushed to the new mesh without interpolation following the scheme proposed in [18].

Numerical simulation of flow is carried out for Re $= 100$ and $KC := \frac{U}{Df} = 5$, where $U = 1$, $D = 1$, $T := 1/f = 5$, and $A = 5/2\pi$. In Figs. 1 and 2, good comparison between the computed solution and experimental data from [40] is shown at two different times that correspond to the phases $7\pi/6$ and $11\pi/6$.

3. Results

In the present work, the needling direction is perpendicular to the skin surface. In practice, it is possible that the needling direction is oblique to the skin surface. The simulation results show that the insertion of an acupuncture needle can influence interstitial fluid flow. The computed velocity field shows that at a location away from the needle, the effect of the stress field on the meshwork vanishes (Fig. 3). Furthermore, when the needle reaches its maximum speed, the interstitial pressure gradient becomes higher at a location close to the needle tip (Fig. 4). The changes in the interstitial fluid flow and the high pressure gradient can affect the activities of the mastocyte pools in the stimulated area. Local mastocyte pools can be activated in regions close to the needle and remain granulated outside this region of triggered mechanical stress.

Another subject of interest is the effects of the fluidic stimuli on an interstitial cell. Local mechanical forces can trigger the activation of mechanoresponsive proteins on the cell surface [20,41] so that Ca^{++} is allowed to enter the cytosol via pressure and shear stress gated ion channels. Simulations are carried out by considering fixed cells and no-slip boundary condition prescribed at the cell surface. Fig. 5 shows the pressure contours on the surface of a cell added closely to the needle. Fig. 6 shows the streamlines and the shear stress along the cell surface. The pressure and the shear stress on the cell surface appear to be higher in the region closest

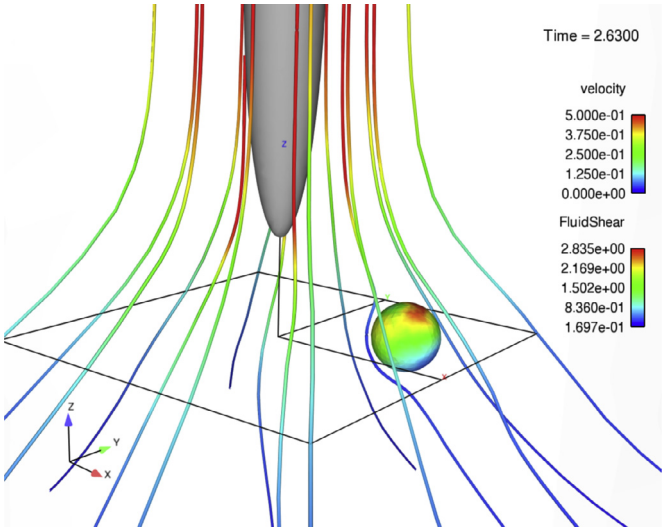

Fig. 6. The predicted streamlines and shear stress on the cell surface as the needle moves toward the cell with $\alpha_f = 0.7$, Da $= 0.321$, and Re $= 0.103$.

to the needle tip. Fluctuation of the pressure and the time varying shear stress suggest that the whole cell surface could be stimulated. Mastocytes have been shown to respond to fluid shear stress [41]. These local mechanical forces participate in the activation of mechanoresponsive proteins on the cell surface [20] so that Ca^{++} is allowed to enter the cytosol via pressure and shear stress gated ion channels.

4. Conclusions

The proposed three-dimensional ALE finite element model is able to describe the interstitial flow and pressure from the macroscopic point of view when a needle is inserted and moved within the hypodermis. High local fluid pressure and shear stress on cells are most likely to appear near the needle tip region. However, the

proposed method does not model the deformation of the extracellular matrix and only the effect of interstitial flow is considered. When considering the rotation of the needle, a large deformation of tissues is observed with the twisting of the fibers around the needle, that in turn makes the corresponding change in interstitial flow. A fluid/structure model taking into account the mechanics of the fibers should then be considered. This study has shown that the numerical prediction of the interstitial pressure and shear stress is an essential tool to gain a better understanding of the activity involved in acupuncture needling.

References

[1] Peskin CS. Numerical analysis of blood flow in the heart. J Comput Phys 1977;25(3):220–52.
[2] Glowinski R, Pan T-W, Periaux J. A fictitious domain method for dirichlet problem and applications. Comput Methods Appl Mech Eng 1994;111(3–4):283–303.
[3] Janela J, Lefebvre A, Maury B. A penalty method for the simulation of fluid-rigid body interaction. In: ESAIM: Proceedings, 14. EDP Sciences; 2005. p. 115–23.
[4] Lefebvre A. Fluid-particle simulations with FreeFem++. In: ESAIM: Proceedings, 18. EDP Sciences; 2007. p. 120–32.
[5] Miller K. Moving finite elements. II. SIAM J Numer Anal 1981;18(6):1033–57.
[6] Miller K, Miller R. Moving finite elements. I. SIAM J Numer Anal 1981;18(6):1019–32.
[7] Liao G, Anderson D. A new approach to grid generation. Appl Anal 1992;44(3-4):285–98.
[8] Cao W, Huang W, Russell R. A moving mesh method based on the geometric conservation law. SIAM J Sci Comput 2002;24(1):118–42.
[9] Tezduyar TE, Behr M, Mittal S, Liou J. A new strategy for finite element computations involving moving boundaries and interfaces – The deforming-spatial–domain/space-time procedure: II. Computation of free-surface flows, two-liquid flows, and flows with drifting cylinders. Comput Methods Appl Mech Eng 1992;94(3):353–71.
[10] Pironneau O, Liou J, Tezduyar T. Characteristic-Galerkin and Galerkin/least-squares space-time formulations for the advection-diffusion equation with time-dependent domains. Comput Methods Appl Mech Eng 1992;100(1):117–41.
[11] Tezduyar TE. Computation of moving boundaries and interfaces and stabilization parameters. Int J Numer Methods Fluids 2003;43(5):555–75.
[12] Takizawa K, Tezduyar TE. Multiscale space–time fluid–structure interaction techniques. Comput Mech 2011;48(3):247–67.
[13] Hirt CW, Amsden AA, Cook JL. An arbitrary Lagrangian-Eulerian computing method for all flow speeds. J Comput Phys 1974;14(3):227–53.
[14] Hughes TJR, Liu WK, Zimmermann TK. Lagrangian-Eulerian finite element formulation for incompressible viscous flows. Comput Methods Appl Mech Eng 1981;29(3):329–49.
[15] Donea J, Giuliani S, Halleux JP. An arbitrary Lagrangian–Eulerian finite element method for transient dynamic fluid-structure interactions. Comput Methods Appl Mech Eng 1982;33(1–3):689–723.
[16] Grandmont C, Maday Y. Fluid-structure interaction: a theoretical point of view. Revue Européenne des Éléments 2000;9(6–7):633–53.
[17] Quarteroni A, Tuveri M, Veneziani A. Computational vascular fluid dynamics: problems, models and methods. Comput Visual Sci 2000;2(4):163–97.
[18] Decoene A, Maury B. Moving meshes with FreeFem++. J Numer Math 2013;20:195.
[19] Deleuze Y, Thiriet M, Sheu TWH. Modeling and simulation of local physical stress on the mastocytes created by the needle manipulation during acupuncture. Commun Comput Phys 2015;18(4):850–67.
[20] Thiriet M. Intracellular Signaling Mediators in the Circulatory and Ventilatory Systems. Biomathematical and Biomechanical Modeling of the Circulatory and Ventilatory Systems, 4. New York, NY: Springer New York; 2013.
[21] Thiriet M, Deleuze Y, Sheu TW. A biological model of acupuncture and its derived mathematical modeling and simulations. Commun Comput Phys 2015;18(4):831–49.
[22] Swartz MA, Fleury ME. Interstitial flow and its effects in soft tissues. Annu Rev Biomed Eng 2007;9(1):229–56.
[23] Park JY, Yoo SJ, Patel L, Lee SH, Lee S-H. Cell morphological response to low shear stress in a two-dimensional culture microsystem with magnitudes comparable to interstitial shear stress. Biorheology 2010;47(3):165–78.
[24] Tseng Y-H, Huang H. An immersed boundary method for endocytosis. J Comput Phys 2014;273:143–59.
[25] Thiriet M. Cell and Tissue Organization in the Circulatory and Ventilatory Systems. Biomathematical and Biomechanical Modeling of the Circulatory and Ventilatory Systems, 1. New York, NY: Springer New York; 2011.
[26] Blasselle A. Modélisation mathématique de la peau, Paris, France: Université Pierre et Marie Curie; 2011. Thèse de doctorat.
[27] Yao W, Ding GH. Interstitial fluid flow: simulation of mechanical environment of cells in the interosseous membrane. Acta Mechanica Sinica 2011;27(4):602–10.
[28] Yao W, Li Y, Ding G. Interstitial fluid flow: the mechanical environment of cells and foundation of meridians. Evidence-Based Complementary Altern Med 2012;2012:1–9.
[29] Thiriet M. Biology and Mechanics of Blood Flows: Part I: Biology. CRM Series in Mathematical Physics. Springer, NY; 2008.
[30] Thiriet M. Cells and tissues. In: Cell and Tissue Organization in the Circulatory and Ventilatory Systems. No. 1. In: Biomathematical and Biomechanical Modeling of the Circulatory and Ventilatory Systems. Springer New York; 2011. p. 11–67.
[31] Hsu CT, Cheng P. Thermal dispersion in a porous medium. Int J Heat Mass Transfer 1990;33(8):1587–97.
[32] Nithiarasu P, Seetharamu KN, Sundararajan T. Natural convective heat transfer in a fluid saturated variable porosity medium. Int J Heat Mass Transfer 1997;40(16):3955–67.
[33] Vafai K, Tien CL. Boundary and inertia effects on flow and heat transfer in porous media. Int J Heat Mass Transfer 1981;24(2):195–203.
[34] Pedersen JA, Boschetti F, Swartz MA. Effects of extracellular fiber architecture on cell membrane shear stress in a 3d fibrous matrix. J Biomech 2007;40(7):1484–92.
[35] Hecht F. New development in FreeFem++. J Numer Math 2013;20(3–4):251.
[36] Fernández MA, Formaggia L, Gerbeau J-F, Quarteroni A. The Derivation of the Equations for Fluids and Structure. In: Formaggia L, Quarteroni A, Veneziani A, editors. Cardiovascular Mathematics. No. 1. MS&A. Springer Milan; 2009. p. 77–121.
[37] Chorin AJ. A numerical method for solving incompressible viscous flow problems. J Comput Phys 1967;2(1):12–26.
[38] Témam R. Une méthode d'approximation de la solution des équations de Navier–Stokes. Bulletin de la Société Mathématique de France 1968;96:115–52.
[39] Raviart P-A, Thomas J-M. Introduction À L'analyse Numérique Des Équations Aux Dérivées Partielles. Masson; 1983.
[40] Dütsch H, Durst F, Becker S, Lienhart H. Low-Reynolds-number flow around an oscillating circular cylinder at low Keulegan–Carpenter numbers. J Fluid Mech 1998;360:249–71.
[41] Wei F, Shi X, Chen J, Zhou L. Fluid shear stress-induced cytosolic calcium signalling and degranulation dynamics in mast cells. Cell Biology International Reports 2012;19(2):45–51.